

PHL 417: a zirconium-rich pulsating hot subdwarf (V366 Aquarid) discovered in *K2* data

R. H. Østensen,^{1,2,3} C. S. Jeffery¹,⁴★ H. Saio,⁵ J. J. Hermes,⁶ J. H. Telting,⁷ M. Vučković,⁸ J. Vos,⁹ A. S. Baran¹² and M. D. Reed¹³

¹Recogito AS, Storgaten 72, N-8200 Fauske, Norway

²ARDASTELLA Research Group, Institute of Physics, Pedagogical University of Krakow, ul. Podchorążych 2, PL-30-084 Kraków, Poland

³Department of Physics, Astronomy, and Materials Science, Missouri State University, Springfield, MO 65897, USA

⁴Armagh Observatory and Planetarium, College Hill, Armagh BT61 9DG, UK

⁵Astronomical Institute, School of Science, Tohoku University, Sendai 980-8578, Japan

⁶Department of Astronomy, Boston University, 725 Commonwealth Ave., Boston, MA 02215, USA

⁷Nordic Optical Telescope, Rambla José Ana Fernández Pérez 7, E-38711 Breña Baja, Spain

⁸Departamento de Física y Astronomía, Universidad de Valparaíso, Avenida Gran Bretaña 1111, Valparaíso 2360102, Chile

⁹Institut für Physik und Astronomie, Universität Potsdam, Karl-Liebknecht-Str 24/25, D-14476 Golm, Germany

Accepted 2020 October 5. Received 2020 September 16; in original form 2020 June 3

ABSTRACT

The *Kepler* spacecraft observed the hot subdwarf star PHL 417 during its extended *K2* mission, and the high-precision photometric light curve reveals the presence of 17 pulsation modes with periods between 38 and 105 min. From follow-up ground-based spectroscopy, we find that the object has a relatively high temperature of 35 600 K, a surface gravity of $\log g/\text{cm s}^{-2} = 5.75$ and a supersolar helium abundance. Remarkably, it also shows strong zirconium lines corresponding to an apparent +3.9 dex overabundance compared with the Sun. These properties clearly identify this object as the third member of the rare group of pulsating heavy-metal stars, the V366-Aquarii pulsators. These stars are intriguing in that the pulsations are inconsistent with the standard models for pulsations in hot subdwarfs, which predicts that they should display short-period pulsations rather than the observed longer periods. We perform a stability analysis of the pulsation modes based on data from two campaigns with *K2*. The highest amplitude mode is found to be stable with a period drift, \dot{P} , of less than $1.1 \times 10^{-9} \text{ s s}^{-1}$. This result rules out pulsations driven during the rapid stages of helium flash ignition.

Key words: stars: abundances – stars: chemically peculiar – stars: fundamental parameters – stars: individual: PHL 417 – stars: oscillations – subdwarfs.

1 INTRODUCTION

Hot subdwarf stars are the evolved remnants of stars that have passed beyond the main-sequence and red-giant-branch stages of evolution, and through one of several possible mass-loss mechanisms they have lost most of their hydrogen envelopes. They are found in significant numbers between the main sequence and the white-dwarf cooling track in the Hertzsprung–Russell diagram. The bulk of their population is made up of the extreme-horizontal-branch (EHB) stars, whose progenitors ignited helium through the core-helium flash, but other stars also reach the hot-subdwarf population either through interaction with a companion or through a merger of two low-mass white dwarfs (see Heber 2009, 2016, for reviews).

B-type hot subdwarf (sdB) stars pulsate with short (p mode: 2–10 m) and long (g modes: 30–120 m) periods. Driving is due to an opacity bump (κ -mechanism) associated with a local overabundance of iron-group elements at temperatures around $2 \times 10^5 \text{ K}$ which results from competition between radiative levitation and gravitational settling (Charpinet et al. 1997a; Fontaine et al. 2003; Jeffery & Saio

2006). The hotter, short-period pulsators are known as V361-Hya stars after the prototype (Kilkenny et al. 1997), and the cooler long-period pulsators as V1093-Her stars (Green et al. 2003). Pulsations have also been detected in the much hotter sdO stars, but the only pulsators of this type found in the field are the prototype, V499 Ser (Woudt et al. 2006), and EO Ceti (Koen 1998; Østensen et al. 2012). These helium-poor sdO stars are thought to be post-EHB stars, since core-helium-burning sdB stars are expected to move to hotter temperatures as they start to run out of helium in their core, and enter a shell-helium-burning phase. The pulsations in these stars is not considered to be problematic, since the same κ -mechanism is expected to operate in this stage, as long as radiative levitation is allowed to work and establish an iron-group-element opacity bump in the driving region (Fontaine et al. 2008). As shell-helium-burning ceases, post-EHB stars contract and move towards the white-dwarf cooling curve, with increasingly short natural frequencies. One sdO star with extremely short pulsation periods ($\sim 30 \text{ s}$) may be the first example (Kilkenny, Worters & Østensen 2017), and could represent the first detected post-EHB DAO pulsator, predicted to be excited by the ϵ -mechanism associated with H-shell burning by Charpinet et al. (1997b).

For a long time, the most mysterious hot-subdwarf variable has been the long-period intermediate helium sdB star

* E-mail: simon.jeffery@armagh.ac.uk

LS IV–14°116 = V366 Aqr, which was discovered to be a long-period pulsator by Ahmad & Jeffery (2005). Whilst subdwarf B stars have predominantly hydrogen-rich surfaces, sdO stars show surfaces ranging from hydrogen-rich to extremely hydrogen-poor. The latter are often classified He-sdO. Naslim et al. (2010) identified a group of subdwarfs having intermediate surface-helium enrichment, i.e. between 10 per cent and 90 per cent helium by number. Most lie close to the sdO/sdB boundary and have thus been variously referred to as intermediate helium subdwarfs, iHe-sdOs and iHe-sdBs.

Ahmad & Jeffery (2005) and Green et al. (2011) recognized that the periods observed in LS IV–14°116 were incompatible with the same (Fe-group) κ -mechanism responsible for pulsations in V361-Hya and V1093-Her pulsators. A spectroscopic study by Naslim et al. (2011) revealed that it was not only somewhat enriched in helium, but found it to have a number of unusual absorption lines from germanium, strontium, yttrium, and zirconium in its optical spectrum, detected at abundances as high as 10 000 times solar. Other examples of such *heavy-metal* stars were later identified (Naslim et al. 2013). Miller Bertolami, Córscico & Althaus (2011) proposed that an ϵ -mechanism present during the core-helium flash ignition phase, rather than the normal κ -mechanism could be responsible for driving the pulsations in V366 Aqr (see also Battich et al. 2018). Recently, Miller Bertolami et al. (2020) have proposed stochastic excitation by convection generated by the same rapid core-helium flashes as an alternative. Both driving mechanisms require the star to be in the pre-EHB phase.

A second object with pulsations similar to V366 Aqr was discovered by Latour, Dorsch & Heber (2019b); Feige 46. This star has a similar atmosphere to the prototype (Latour, Green & Fontaine 2019a). Its pulsation periods (2200–3400 s) overlap the range found for V366 Aqr (Green et al. 2011, 1950–5100 s). Subsequently, Saio & Jeffery (2019) showed that the κ -mechanism operating through carbon and oxygen opacities at ~ 1 million K could account for the pulsations in both LS IV–14°116 and Feige 46, but only if carbon and/or oxygen abundances are substantially enhanced at these temperatures.

In this paper, we present the third object of the V366-Aqr class of pulsators, PHL 417, and the first such object observed with space-based photometry.

2 K2 OBSERVATIONS

The target of the current paper was first catalogued as PHL 417 from the survey of Haro & Luyten (1962), where it is identified as a faint blue star with a photographic magnitude $B = 16.9$, and colours $B - V = -0.2$, $U - B = -0.4$. It appears in the SDSS catalogue (Stoughton et al. 2002) as SDSS J231105.09–013706.0 with $ugriz = 16.22, 16.52, 17.01, 17.37, 17.68$. It was based on these colours that it was selected as a candidate WD pulsator and proposed as a short-cadence target for the *K2* mission, where it was designated EPIC 246373305 in the Ecliptic Plane Input Catalogue (Huber et al. 2016). The Gaia DR2 catalogue has this star with $G = 16.792(2)$ and a parallax of 0.48(9) mas (Gaia Collaboration 2018).

PHL 417 was observed in short cadence (SC) during Campaigns 12 and 19 of the *K2* mission. C12 observations started on 2016 December 15 and ended on 2017 March 4, with a 5-d gap in the 79 d run. The gap, which occurred around 2/3 of the way through the campaign, was not large enough to produce significant multipeak structure in the window function. C19 ran from 2018 September 8 to 23, when the spacecraft ran out of propellant.

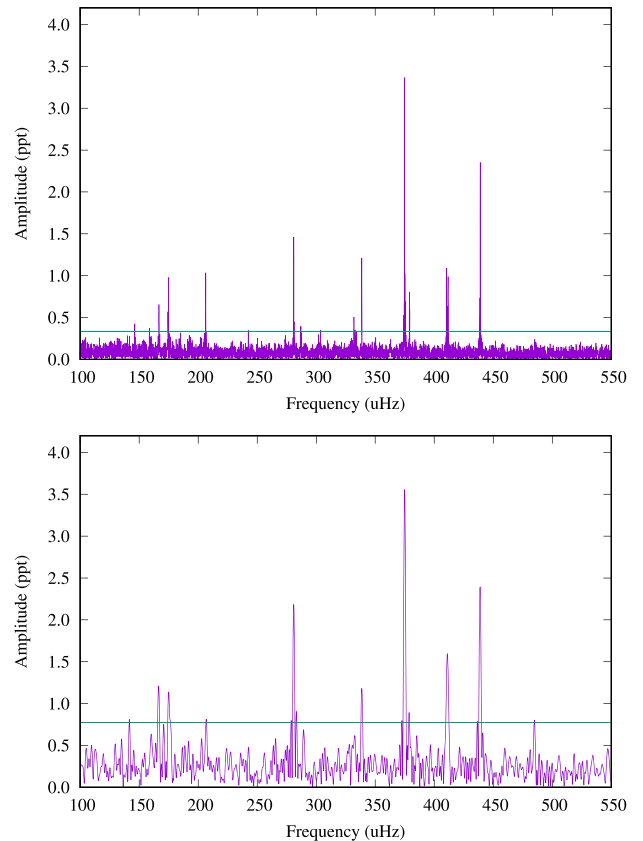


Figure 1. Amplitude spectra of the K2 data sets of PHL 417 up to 550 μHz for C12 (upper panel) and C19 (lower panel). The green line indicates the detection threshold (see text for details).

For C12, target pixel files were downloaded from the ‘Barbara A. Mikulski Archive for Space Telescopes’ (MAST),¹ since no pipeline processed SC light curves were available at the time. The pixel files were processed by first using standard IRAF tasks to extract fluxes, and then using custom Python scripts to decorrelate fluxes in X and Y directions around a 2D mask for the target to remove the light-curve effects caused by the spacecraft’s thruster firings. For C19, the pipeline-processed SC light curve was used. This light curve covers only 7.25 d of the C19 campaign. During the first part of the campaign, the pointing of the telescope was off, and during the last part, the pointing was too erratic to recover useful data. The usable data are sufficient to verify the frequencies found in C12.

The Fourier transform (FT) of the resulting light curve is shown in Fig. 1. A number of significant peaks are clearly seen in the low-frequency region of the FT. By corollary with analyses of light curves of other hot subdwarfs, where pulsations were established independently from light and velocity variations, and from theoretical models, the multip peaked FT of the *K2* light curve of PHL 417 is strongly suggestive of the multiperiod non-radial oscillations seen in V1093-Her variables.

The RMS σ in the featureless frequency region between 1000 and 2000 μHz was measured to be 0.072 parts per thousand (ppt) and 0.192 ppt for C12 and C19, respectively. This indicates the noise level and is representative for the region where significant frequencies are found. The noise increases slightly at the lowest frequencies. The

¹archive.stsci.edu.

Table 1. Peaks detected in the Fourier transform of the K2 light curve of PHL 417.

ID	Frequency (μHz)	Period (s)	Amplitude (ppt)
f_1	146.291(11)	6835.7	0.42(6)
f_2	158.589(13)	6305.6	0.43(-)
f_3	166.747(7)	5997.1	0.66(6)
f_4	174.750(5)	5722.5	0.97(6)
f_5	206.418(5)	4844.6	1.04(6)
f_6	242.410(14)	4125.2	0.35(6)
f_7	280.973(3)	3559.0	1.47(6)
f_8	286.990(-)	3484.4	0.40(-)
f_9	303.630(13)	3293.5	0.35(6)
f_{10}	331.960(9)	3012.4	0.50(6)
f_{11}	332.939(13)	3003.6	0.37(6)
f_{12}	338.431(7)	2954.8	0.74(6)
f_{13}	338.606(4)	2953.3	1.25(6)
f_{14}	374.914(1)	2667.3	3.39(6)
f_{15}^-	378.896(7)	2639.3	0.74(6)
f_{15}^+	379.233(10)	2636.9	0.53(6)
f_{16}^-	410.403(4)	2436.7	1.12(6)
f_{16}^0	411.064(7)	2432.8	0.66(6)
f_{16}^+	411.702(5)	2428.9	0.90(6)
f_{17}	438.941(2)	2278.2	2.35(6)

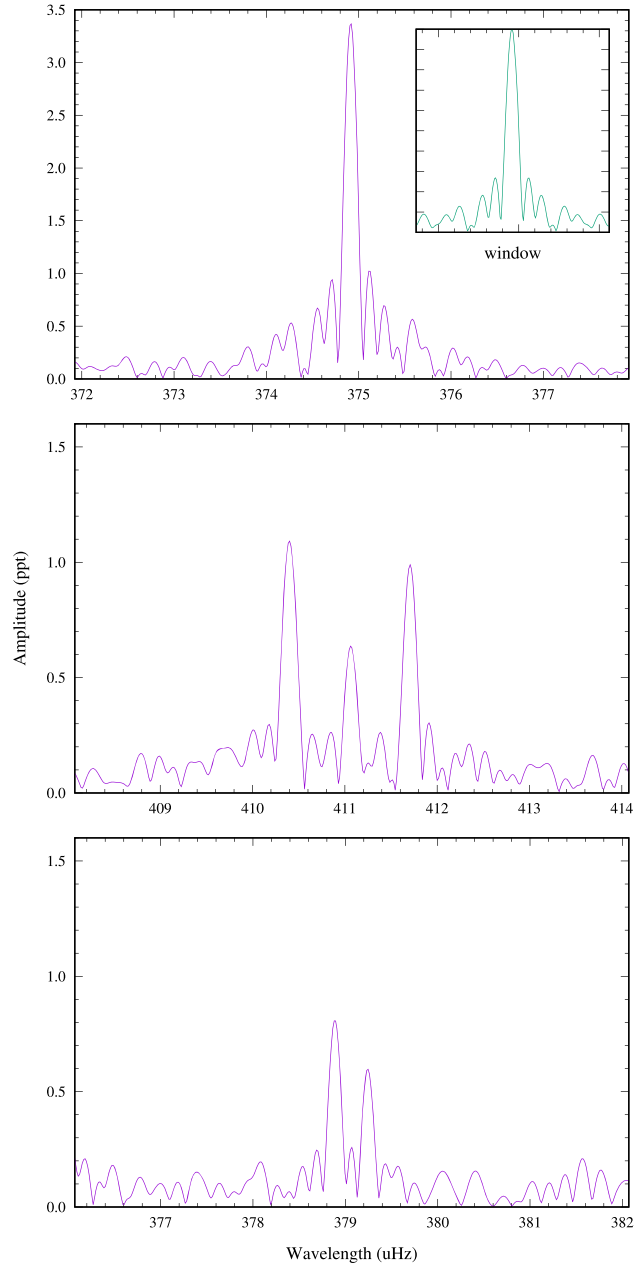
light curves have $n = 104\,542$ (C12) and $10\,466$ (C19) good data points. For a normal distribution, the 1-in- n chance of a spurious detection σ should be 4.43 (C12) and 3.9 (C19). Detection thresholds of 4.5σ and 4.0σ were adopted for the two data sets, i.e. 0.33 and 0.77 ppt, respectively.

Taking into account the difference in sampling and resolution, the two FTs are almost identical. The only difference is a peak at $484.8\ \mu\text{Hz}$ which is significant in C19 and only just detectable in C12. It is evident from Fig. 1 that the pulsator is very stable over the two runs. When taking into account that the apertures are somewhat different, and that the background flux may be different, the amplitudes of the main peaks can easily be the same within the errors.

We summarize the result of the frequency analysis in Table 1. Two of the peaks in the FT show multiple components (Fig. 2). If due to non-radial oscillations, the multiplets could be consistent with sectoral modes having $\ell = 1$ and 2. The triplet (f_{16}) around $411\ \mu\text{Hz}$ shows a symmetric splitting of $0.66\ \mu\text{Hz}$. The doublet (f_{15}) at $379\ \mu\text{Hz}$ shows a split of $0.34\ \mu\text{Hz}$. As this is the narrowest splitting, it most likely corresponds to an $\ell = 1$ g mode, which would have a normal Ledoux constant $C_{\text{nl}} = 0.5$, and corresponding to a rotation period of ~ 17 d. Under conservative assumptions for the radius, this corresponds to an equatorial velocity of $\sim 0.5\ \text{km s}^{-1}$, so PHL 417 appears to be a slow rotator, just like LS IV-14°116 and Feige 46 (Naslim et al. 2011; Latour et al. 2019b). Without detecting more multiplets, direct mode identification is not possible from rotational frequency splitting.

The period spacing between modes of the same ℓ and consecutive radial order has been shown to follow the expected asymptotic sequences with even period spacing of ~ 250 s in almost all V1093-Her stars observed with *Kepler*. Although the main mode and the triplet show a spacing of 234 s, the sequence is not found to continue, and no other even spacing can be found.

The only dB pulsators in the temperature region above 35 kK with high-quality space data are KIC 10139564, observed during the main *Kepler* mission (Baran et al. 2012), and the *K2* target PG 1315-123 (Reed et al. 2019). While both these stars are predominantly p-mode

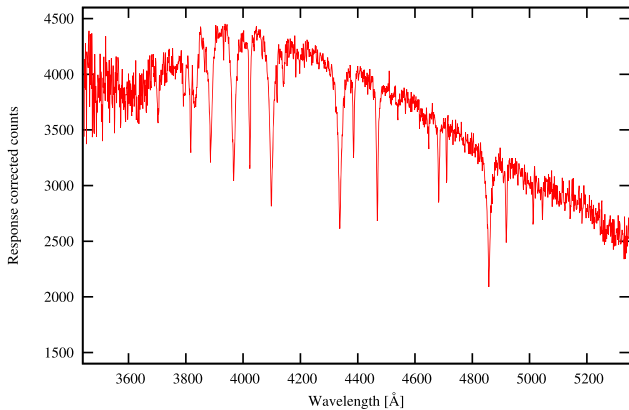
**Figure 2.** Expanded sections of the FT of the C12 light curve of PHL 417: the largest-amplitude peak (f_{14} ; top), a triplet (f_{16} ; middle), and a doublet (f_{15} ; bottom). The window function is shown inset in the top panel.

pulsators, they also show a fair number of pulsation periods in the range 1500–4000 s, which overlaps with the period range found in PHL 417. Unlike the periods of the cooler V1093-Her stars, which form evenly spaced sequences as predicted by theoretical models, the periods in KIC 10139564 and PG 1315-123 do not follow any clearly evenly spaced sequences, just as we see for PHL 417.

Of particular interest is the phase stability of the pulsation modes, since modes driven by the ϵ -mechanism have been predicted to be changing at a rate of $\dot{P} \approx 10^{-7}$ to 10^{-4} (Battich et al. 2018). We can divide the *K2* data sets into chunks roughly 1 week long each, and measure how frequency and phase change in time. Not one of the modes that have significant amplitudes in the individual chunks shows any sign of a clear drift. This becomes even more evident

Table 2. Log of spectroscopic observations.

Date-time (UT start)	Exp (s)	S/N	Telescope/inst.
2017-08-12 04:38:21	900	23	NOT/ALFOSC
2017-08-13 01:58:00	900	34	NOT/ALFOSC
2017-08-14 01:02:20	900	31	NOT/ALFOSC
2017-08-20 05:06:49	900	26	NOT/ALFOSC
2017-09-18 05:19:52	1200	64	Magellan/MagE
2017-09-18 05:40:16	1200	64	Magellan/MagE
2017-09-18 06:00:39	1200	60	Magellan/MagE
2017-09-19 23:40:40	900	42	NOT/ALFOSC
2017-09-30 22:03:55	900	27	NOT/ALFOSC
2017-10-11 00:56:59	900	29	NOT/ALFOSC
2017-10-11 01:31:31	900	34	NOT/ALFOSC

**Figure 3.** Sum of the eight NOT/ALFOSC spectra.

when including the C19 data to the picture. For all modes detected in C19, the C19 period is found to be well within the spread of the measurements from the C12 chunks. The modes that give the clearest constraint are the highest amplitude modes. For f_{14} , we see that any change must be slower than $1.1 \times 10^{-9} \text{ s s}^{-1}$, and for f_{17} we get a limit of $3.0 \times 10^{-9} \text{ s s}^{-1}$. These numbers are calculated using 3σ uncertainties from a quadratic fit to the observed phase evolution (O–C diagram) for f_{14} and f_{17} .

3 SPECTROSCOPY

Following notification of sdB-like pulsations, PHL 417 was added to the spectroscopic *Kepler* sdB follow-up survey (Telting et al. 2012). The survey uses the ALFOSC spectrograph on the 2.6-m Nordic Optical Telescope (NOT), with grism #18 and an 0.5-arcsec slit, giving a resolution $R = 2000$, which corresponds to 2.2 \AA full width at half-maximum (FWHM). Eight spectra of PHL 417 were obtained between 2017 August 3 and 2017 October 11 (Table 2), and are more than sufficient to identify any orbital acceleration. The data are consistent with no radial velocity variations, within the time-scale covered by the observations, which is too short to rule out long-period binarity with time-scales of the order of 100 d or more. The median radial velocity error of the data set is 3.5 km s^{-1} , when using the sharper He lines rather than the Balmer lines. After applying heliocentric corrections, the spectra were co-added to yield a mean spectrum with an S/N peaking at ≈ 83 at 4000 \AA (Fig. 3). The radial velocity of the mean spectrum, as measured from He I lines, is $-63 \pm 5 \text{ km s}^{-1}$. A systematic zero-point error of 10 km s^{-1} is appropriate for ALFOSC.

The NOT/ALFOSC spectrum of PHL 417 does not show the typical V1093-Her spectrum expected from initial analysis of the light curve. On the contrary, both neutral and ionized helium are strong. A preliminary analysis of the first spectrum showed effective temperature (T_{eff}), surface gravity (g), and surface helium abundance ($y = n_{\text{He}}/n_{\text{H}}$) all too high for PHL 417 to be a V1093-Her variable, and indicated that the spectrum is similar to that of the helium sdB pulsators LS IV–14° 116 (Naslim et al. 2011) and Feige 46 (Latour et al. 2019b). This prompted follow-up spectroscopy using the Magellan Echellette (MagE, Marshall et al. 2008) on the 6.5-m Baade Magellan Telescope on Las Campanas Observatory, Chile. Three spectra with exposures of 1200 s each were obtained on the night of 18 September 2017 with a 1.0 arcsec slit yielding a resolution of $R = 4100$, see Table 2. In addition to the science spectra, the internal quartz and dome flat-field lamps were obtained for pixel response calibration and ThAr lamps spectra were obtained for wavelength calibration. The MagE spectra were reduced using the MASE pipeline (Bochanski et al. 2009) following standard procedures for order tracing, flat-field correction, wavelength calibration, and optimal source extraction. The extracted spectrum (each order) was divided by the blaze function, which is obtained from the flat-field frames. Given the differences in the continuum of the observed star and the blaze correcting function (obtained for the flat) the deblazed orders will inevitably have a certain slope (smooth variation) that will not reflect the shape of the continuum of the observed star. Therefore, we have continuum normalized each order by fitting a low-order polynomial to the deblazed flux including an iterative procedure that excludes absorption lines from the fit. Once the orders were continuum normalized they were co-added in a single spectrum. For the overlapping edges of sequential orders, the average was computed. The spectrum analyzed is the sum of 3×1200 s exposures and has a S/N ≈ 100 at 4750 \AA and wavelength coverage $3080\text{--}8280 \text{ \AA}$.

Photospheric parameters were measured from both the NOT/ALFOSC and MagE spectra using methods described by Jeffery & Miszalski (2019).

The Armagh LTE radiative transfer package LTE-CODES (Jeffery, Woolf & Pollacco 2001; Behara & Jeffery 2006) includes a model atmosphere code STERNE, a formal solution code SPECTRUM and a general purpose fitting package SFIT.² Effective temperature, surface gravity, and surface helium and hydrogen abundances were obtained by finding the best-fitting spectrum in a grid of models. To improve on any normalization carried out during data reduction, a high-pass filter is applied during the fit, following the steps described by Jeffery et al. (1998). A broad enough filter is chosen so as not to degrade the gravity-sensitive line wings. The preliminary ALFOSC fit cross-checks that this has been applied correctly.

For both spectra we use a grid³ covering a parameter space with

$$[T_{\text{eff}}/\text{kK}, \log g/\text{cm s}^{-2}, n_{\text{He}}] \\ = [28(02)40, 5.0(0.25)6.25, 0.1(0.1)0.3(0.2)0.90],$$

sampled over the wavelength interval $3400\text{--}7100 \text{ \AA}$, and which assumed an abundance distribution for elements heavier than helium based on a mean for hot subdwarfs compiled by Pereira (2011), but simplified for the STERNE input to 1/10 solar for $2 < Z < 26$ and solar for $Z \geq 26$ (Naslim, Jeffery & Woolf 2020). A microturbulent

²Local thermodynamic equilibrium was assumed throughout the analysis.

³In this notation, the grid is defined by three parameters $[p_1, p_2, p_3]$ and three triplets $p_{\text{min}}(\delta p)p_{\text{max}}$ implying $p \in p_{\text{min}}, p_{\text{min}} + \delta p, p_{\text{min}} + 2\delta p, \dots, p_{\text{max}}$. Additional terms are added if the grid step δp changes.

Table 3. Atmospheric parameters for PHL 417 obtained from spectra observed with ALFOSC and MagE. Parentheses show statistical errors in the last digit(s). Systematic errors due to observation can be estimated by comparing the two sets of measurements.

Solution	ALFOSC	MagE
T_{eff} (kK)	35.35(6)	35.92(4)
$\log g$ (cm s^{-2})	5.73(1)	5.74(1)
n_{He}	0.232(3)	0.259(3)
$\log y$	-0.520(2)	-0.457(2)

velocity $v_{\text{turb}} = 5 \text{ km s}^{-1}$ was assumed for both the calculation of line opacities in the model atmosphere calculation (which affects the temperature stratification of the models) and for the formal solution, which affects relative line strengths and widths. Whilst possibly overestimated for the current case, associated systematic errors are small compared with those arising from data quality (Jeffery & Miszalski 2019).

The solutions obtained in each case are given in Table 3 (ALFOSC and MagE). The solution for the NOT/ALFOSC spectrum is shown in Fig. 4. There are systematic differences associated with the different wavelength ranges adopted in the solutions, which mean that different hydrogen and helium lines contribute, in particular, to the surface gravity measurement and hence in turn to the effective temperature and surface helium, since these quantities are not

independent in the solutions. We adopt the mean of the ALFOSC and MagE measurements for comparison with other hot subwarfs, giving $T_{\text{eff}} = 35.64 \pm 0.28 \text{ kK}$, $\log g/\text{cm s}^{-2} = 5.73 \pm 0.01$, and $\log y = -0.49 \pm 0.02$. Errors are a combination of statistical errors in the fit and the difference between ALFOSC and MagE from Table 3.

These measurements are subject to a range of systematic effects, including the adoption of the LTE approximation, the metallicity and microturbulent velocity adopted in the models, the resolution and extent of the model grid, and the methods used to match the overall continuum level. Experiments with different model grids, including one based on zero-metal non-LTE model atmospheres (Németh, Kawka & Vennes 2012), one with a solar distribution of metals, and several with different distributions of grid points, yield results with ranges $\Delta T_{\text{eff}} \approx 1.87 \text{ kK}$, $\Delta \log g \approx 0.33$, and $\Delta \log y \approx 0.04$. Given the quality of the observational data, the above solution is taken to be indicative and we conservatively adopt systematic errors $\delta T_{\text{eff}} \approx 0.75 \text{ kK}$, $\delta \log g \approx 0.15$, and $\delta \log y \approx 0.04$, which we combine quadratically with the statistical errors to give total errors $\Delta T_{\text{eff}} \approx 0.8 \text{ kK}$, $\Delta \log g \approx 0.15$, and $\Delta \log y \approx 0.05$.

4 ABUNDANCES

We computed a model atmosphere close to the MagE solution and proceeded to derive a formal solution having abundances corresponding to the mixture adopted above. Given the pulsation properties, we experimented with increasing the zirconium abundance and

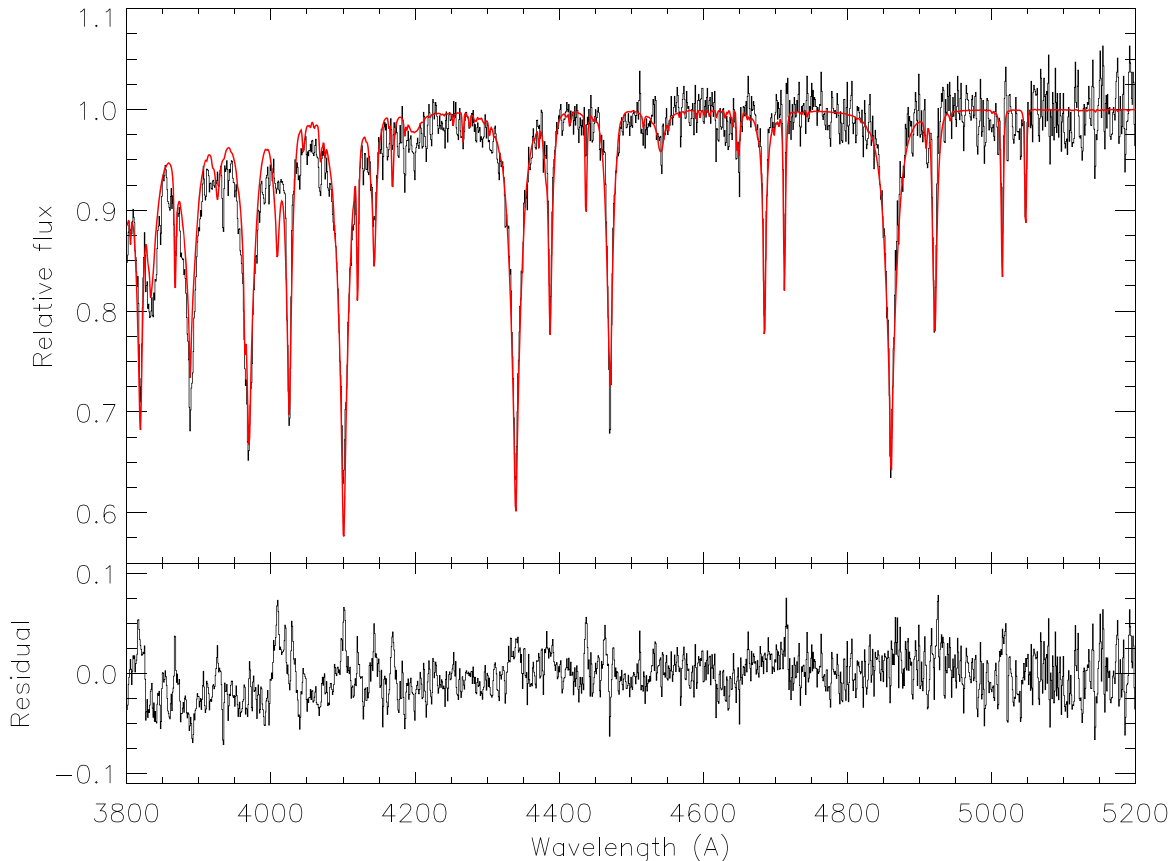


Figure 4. The ALFOSC spectrum of PHL 417 (black histogram: upper panel) and the best-fitting (interpolated) model (red) having $T_{\text{eff}} = 35350 \text{ K}$, $\log g/\text{cm s}^{-2} = 5.73$, and $n_{\text{He}} = 0.23$, $v_{\text{turb}} = 5 \text{ km s}^{-1}$. The model has been degraded to the instrumental resolution. The residual (observed – model) is plotted at the same scale in the lower panel.

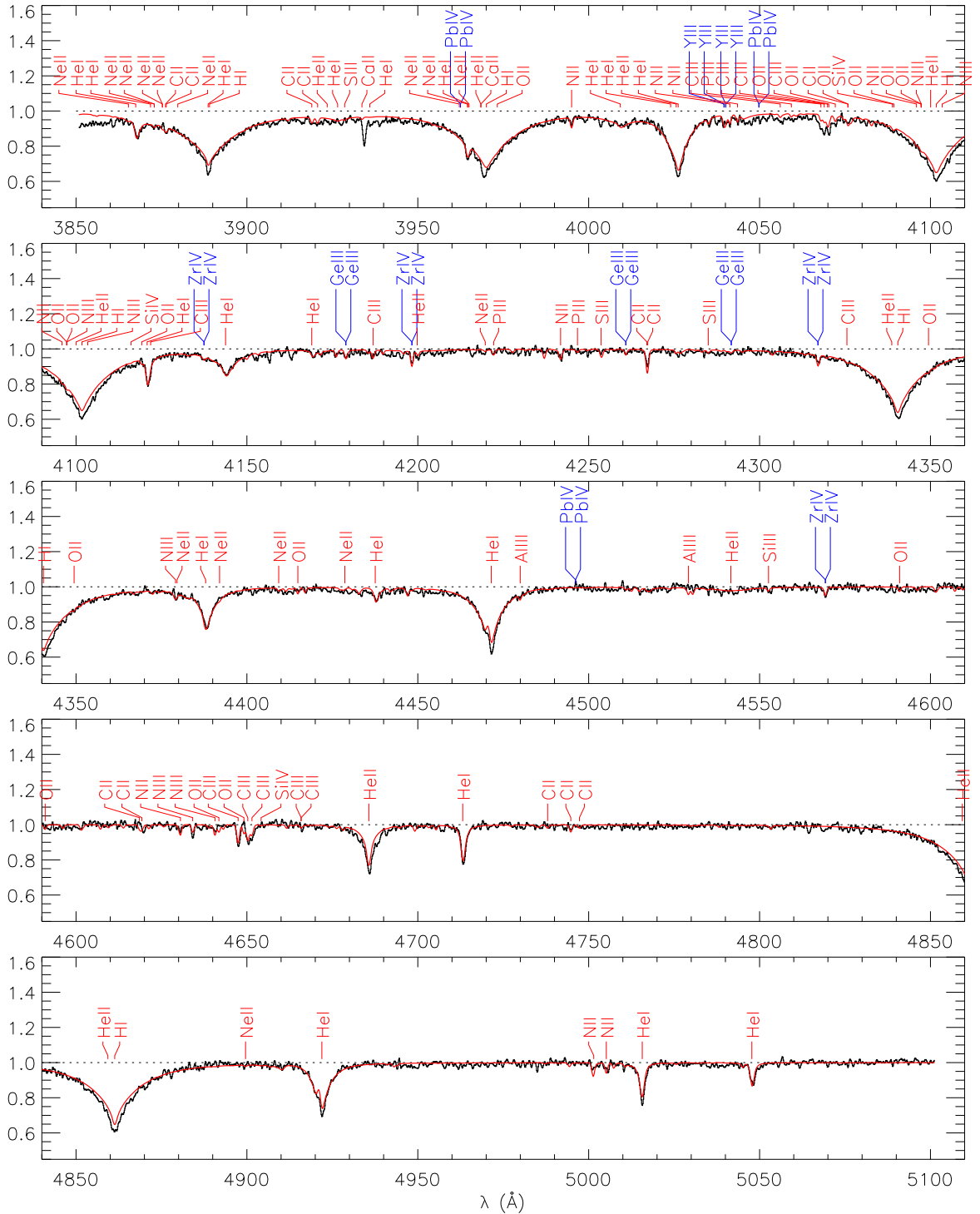


Figure 5. The MagE spectrum of PHL 417 (black histogram) and a model having $T_{\text{eff}} = 35\,600\text{ K}$, $\log g/\text{cm s}^{-2} = 5.750$, $n_{\text{He}} = 0.23$, $v_{\text{turb}} = 5\text{ km s}^{-1}$, and abundances as given in Table 5. The observed spectrum and model have been resampled at a dispersion of $0.15\text{ \AA pixel}^{-1}$. Lines with predicted equivalent widths $> 15\text{ m\AA}$ are labelled. The model is convolved with an instrumental profile of 0.8 \AA (FWHM).

immediately recognized three strong zirconium lines in the MagE spectrum. The resolution and signal-to-noise of the latter are not ideal for abundance analysis. Nevertheless, the presence (or absence) of certain lines can be used to obtain some idea of the surface composition (Fig. 5). Predictably present in the wavelength range 3850–5100 Å are lines of carbon (C II,III), nitrogen (N II,III), oxygen

(O II), neon (Ne II), silicon (Si IV), sulphur (S III), and phosphorous (P III). Also remarkably present are zirconium (Zr IV), germanium (Ge III), and probably yttrium (Y III) (Fig. 6). There was no evidence for lead (Pb IV). Equivalent widths were measured for the strongest lines for all of these species; the threshold is about 12–15 mÅ, and this also represents the typical error on all of the measured equivalent

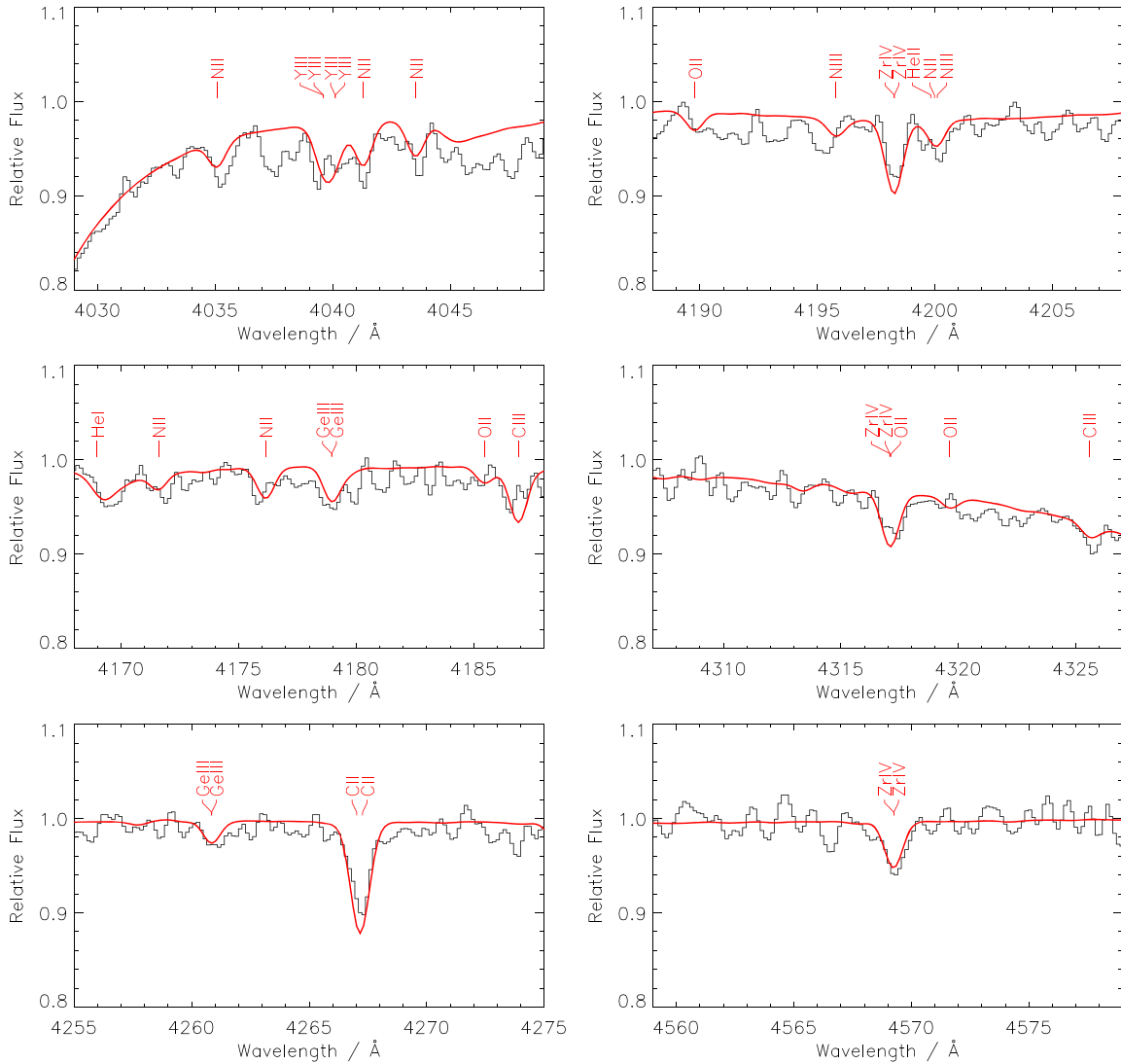


Figure 6. Selected regions of the MagE spectrum of PHL 417 (black histogram) and model (red curve) as shown in Fig. 5 showing the principal yttrium, germanium, and zirconium lines. Other lines with predicted equivalent widths $>10 \text{ m}\text{\AA}$ are labelled.

widths. A model atmosphere was computed corresponding to the final parameters adopted in Table 3. Table 4 shows abundances derived from the measured equivalent widths assuming a micro-turbulent velocity $v_{\text{turb}} = 5 \text{ km s}^{-1}$. Abundances obtained for C II and C III are similar, indicating that equilibrium is satisfied for this pair of ions. A formal solution based on these abundances is shown in Fig. 5. The results are summarized in Table 5, where it is emphasized that these are based on a few strong lines and higher precision measurements are desirable. For comparison, Table 5 also shows the solar abundances for the same species; note that atmospheric carbon and oxygen are depleted in PHL 417 with respect to solar. Statistical errors cited for $\log \epsilon_i$ are derived from equivalent width measurement errors and/or the standard deviation around the mean of multiple line measurements. Systematic errors in $\log \epsilon_i$ propagated from total errors $\delta \log g/\text{cm s}^{-2} \approx 0.15$, $\delta n_{\text{He}} \approx 0.05$, and $\delta v_{\text{turb}} \lesssim 5 \text{ km s}^{-1}$ are all $\lesssim 0.05$. The total error $\delta T_{\text{eff}} \approx 0.8 \text{ kK}$ leads to systematic errors $|\delta \log \epsilon|$ ranging from <0.06 (N, C, Ne) up to ≈ 0.36 (P, Ge) with the remainder ranging from 0.08 to 0.23 (Zr, Y, O, Si, S). The systematic abundance errors are all smaller than the statistical errors.

The preceding analysis shows that PHL 417 belongs to the group of intermediate helium subdwarfs (iHe-sds) as defined by Naslim et al. (2010). These objects distinguish themselves from the main population of sdB stars, which are clearly associated with the EHB, since they produce a narrow band in the $g-T_{\text{eff}}$ diagram (Fig. 7). They are also significantly different from the rather large population of very helium-rich sdO and sdOB stars, which are found in the $g-T_{\text{eff}}$ diagram mostly between ~ 40 and 50 kK without any clustering in g .

Among a number of proposed solutions, one possible explanation for these objects is that they are evolving towards the helium main sequence, or zero-age EHB, and that their low atmospheric H abundance is due to gravitational stratification not having had the time to act since their formation (Naslim et al. 2010, 2011). The intermediate helium stars may represent a transition between these objects, at least for those objects that are found close to the zero-age EHB or He-MS. This is exactly where we find the three V366-Aqr pulsators.

PHL 417 is clearly related to LS IV-14° 116 and Feige 46 as it has similar spectroscopic parameters and surface composition (as far as the data quality permits). The so-called heavy-metal stars all lie

Table 4. Line abundances for PHL 417 derived from the MagE spectrum showing wavelength (λ), adopted oscillator strengths ($\log gf$), equivalent widths (W_λ), and elemental abundances ($\log \epsilon$). The mean error on the equivalent widths is ± 15 mÅ and is propagated to obtain the error on each line abundance. $d\epsilon/dW_\lambda$ depends where on the curve of growth W_λ lies and differs from line to line by large amounts.

Ion	λ (Å)	$\log gf$	W_λ (mÅ)	$\log \epsilon$
C II	4744.77	-0.600	27	7.93 ± 0.31
C II	4267.27	0.734	95	8.17 ± 0.14
C III	4186.90	0.924	39	7.96 ± 0.29
C III	4325.56	0.090	22	8.23 ± 0.45
N II	3995.00	0.225	52	8.03 ± 0.26
N II	5005.15	0.612	66	8.39 ± 0.25
N III	4640.64	0.140	35	7.79 ± 0.34
O II	4075.86	0.693	37	7.83 ± 0.31
O II	4072.15	0.552	28	7.77 ± 0.36
Ne II	3875.28	-0.080	39	7.67 ± 0.24
Si IV	4088.85	0.199	13	5.57 ± 0.67
P III	4222.20	0.210	22	5.99 ± 0.36
S III	4253.59	0.400	15	6.13 ± 0.50
S III	4284.98	0.110	16	6.44 ± 0.47
Ge III	4178.96	0.341	31	5.91 ± 0.30
Ge III	4260.85	0.108	25	6.02 ± 0.35
Y III	4039.60	1.005	48	6.48 ± 0.22
Zr IV	4198.27	0.323	56	6.10 ± 0.20
Zr IV	4317.08	0.069	47	6.24 ± 0.22
Zr IV	4569.25	1.127	59	6.63 ± 0.19
Zr IV	4137.44	-0.625	33	6.68 ± 0.28

Note. C II: Yan, Taylor & Seaton (1987), C III: Hibbert (1976), Hardorp & Scholz (1970), N II: Becker & Butler (1989), N III: Butler (1984), O II: Becker & Butler (1988), Ne II: Wiese, Smith & Glennon (1966), Si IV: Becker & Butler (1990), P III: Wiese et al. (1966), S III: Wiese, Smith & Miles (1969), Ge III: Naslim et al. (2011), Y III: Naslim et al. (2011), Zr IV: Naslim et al. (2011).

close to the EHB/HeMS junction in the $g-T_{\text{eff}}$ diagram. They fall into three distinct groups: (a) the V366 Aquarids, which are rich in germanium, yttrium, and zirconium (solid blue symbols in Fig. 7), (b) a group of about eight stars, including UVO 0825+15, which show very significant overabundances of lead and other elements with $Z \geq 20$, including in some instances, zirconium (solid grey), and (c) a number of other intermediate helium stars with very high overabundances of iron-group elements (open grey).

5 PULSATIONS

The discovery of pulsations in LSIV-14°116 (Ahmad & Jeffery 2005; Green et al. 2011) presented a problem since, with $T_{\text{eff}} \approx 35\,500$ K, the star is too hot for g modes to be driven by Fe + Ni bump opacities. Miller Bertolami et al. (2011) and Battich et al. (2018) have proposed that a nuclear instability in the inward-burning shell of a pre-EHB star can excite pulsations via the ϵ -mechanism.

Again, the difficulty is to drive pulsations in stars with precisely the T_{eff} and g ranges of LSIV-14°116 and, also, Feige 46 (Latour et al. 2019a,b). The pulsations in PHL 417 span the same period range and also have similar amplitudes (0.3–3.3 ppt) to Feige 46 (0.9–2.9 ppt) and LSIV-14°116 (1.0–2.7 ppt) (Green et al. 2011; Latour et al. 2019a). By comparing thermal and dynamical time-scales of models in the correct T_{eff} and g ranges, Saio & Jeffery (2019) proposed that the κ -mechanism would work if there were opacity bumps around 10^6 K. By constructing a class of helium core-burning models in which the abundances of carbon and oxygen are substantially enhanced at these temperatures, Saio & Jeffery (2019) found that g-mode pulsations could be excited in exactly the period ranges observed in LSIV-14°116 and Feige 46.

Following discovery of pulsations in PHL 417 and using the same methods as described in Saio & Jeffery (2019), a new model was constructed having approximately the observed surface properties of PHL 417, an assumed mass of $0.50 M_\odot$, and an interior composition of 40 per cent helium, 30 per cent carbon, and 30 per cent oxygen. Such a structure might arise, for example, if the subdwarf evolved from a relatively massive zero-age helium main-sequence star, after a very rapid mass-loss event due to interaction with a companion in a binary system (Saio & Jeffery 2019). Other metals have scaled-solar ratios with $Z = 0.02$. Considering both dipole ($\ell = 1$) and quadrupole ($\ell = 2$) modes, g modes are excited across the entire period range observed in PHL 417 (Fig. 8).

All three V366 Aqr variables are pure g-mode pulsators with nothing detected in the p-mode regime, even at the photometric sensitivity of *K2*. Note that p modes in these stars are predicted to have periods of less than about 300 s, which would be easily detectable in *Kepler* short-cadence photometry, where the Nyquist limit is around 118 s. The κ -mechanism excitation in an ionization zone is most effective if the period of pulsation is comparable with the thermal time-scale there (e.g. Cox 1974). However, in the models of V366-Aqr variables, p-mode oscillations cannot be excited by the κ -mechanism in helium or C/O ionization zones, because the thermal time-scale is too short (~ 0.1 s) in the helium ionization zone or too long ($\sim 10^3$ – 10^5 s) in the C/O ionization zone.

A feature of the FT presented in Fig. 1 is the relatively high density of g modes and the absence of any asymptotic sequence. Fig. 9 shows an Echelle diagram for PHL 417 with $\ell = 1$ g modes of a $0.5 M_\odot$ model. The observed g-mode density is higher than expected for $\ell = 1$ and two g modes alone. Relatively little else may be concluded except that the observed triplet is most likely a dipole mode.

6 CONCLUSIONS

K2 photometry of PHL 417 has revealed a relatively rich pulsation spectrum in the g-mode region of pulsations in hot subdwarf stars. Follow-up ground-based spectroscopy demonstrates physical parameters and abundances that have allowed us to identify this

Table 5. Atmospheric abundances of PHL 417 and other V366 Aqr variables given as $\log \epsilon$, normalized to $\log \Sigma \mu \epsilon = 12.15$. Errors are given in parentheses. The second line, marked *n*, shows the number of lines contributing to each measurement for PHL 417.

Star	H	He	C	N	O	Ne	Si	P	S	Ge	Y	Zr	Reference
PHL 417	11.77(3)	11.31(3)	8.0(2)	8.1(3)	7.8(2)	7.7(2)	5.6(7)	6.0(4)	6.3(4)	6.0(2)	6.5(2)	6.4(3)	This work
<i>n</i>			4	3	2	1	1	1	2	2	1	4	
LSIV-14°116	11.83(7)	11.15(5)	8.0(2)	8.0(2)	7.6(2)	<7.6	6.3(1)			6.3(1)	6.2(1)	6.5(2)	Naslim et al. (2011)
Feige 46	11.71(2)	11.35(4)	8.6(3)	8.1(1)	7.5(2)	–	5.6(1)		<5.9(3)	5.8(6)	6.5(4)	6.6(1)	Latour et al. (2019b)
Sun	12.00	10.93	8.4	7.8	8.7	7.9	7.5	5.4	7.1	3.7	2.0	2.6	Asplund et al. (2009)

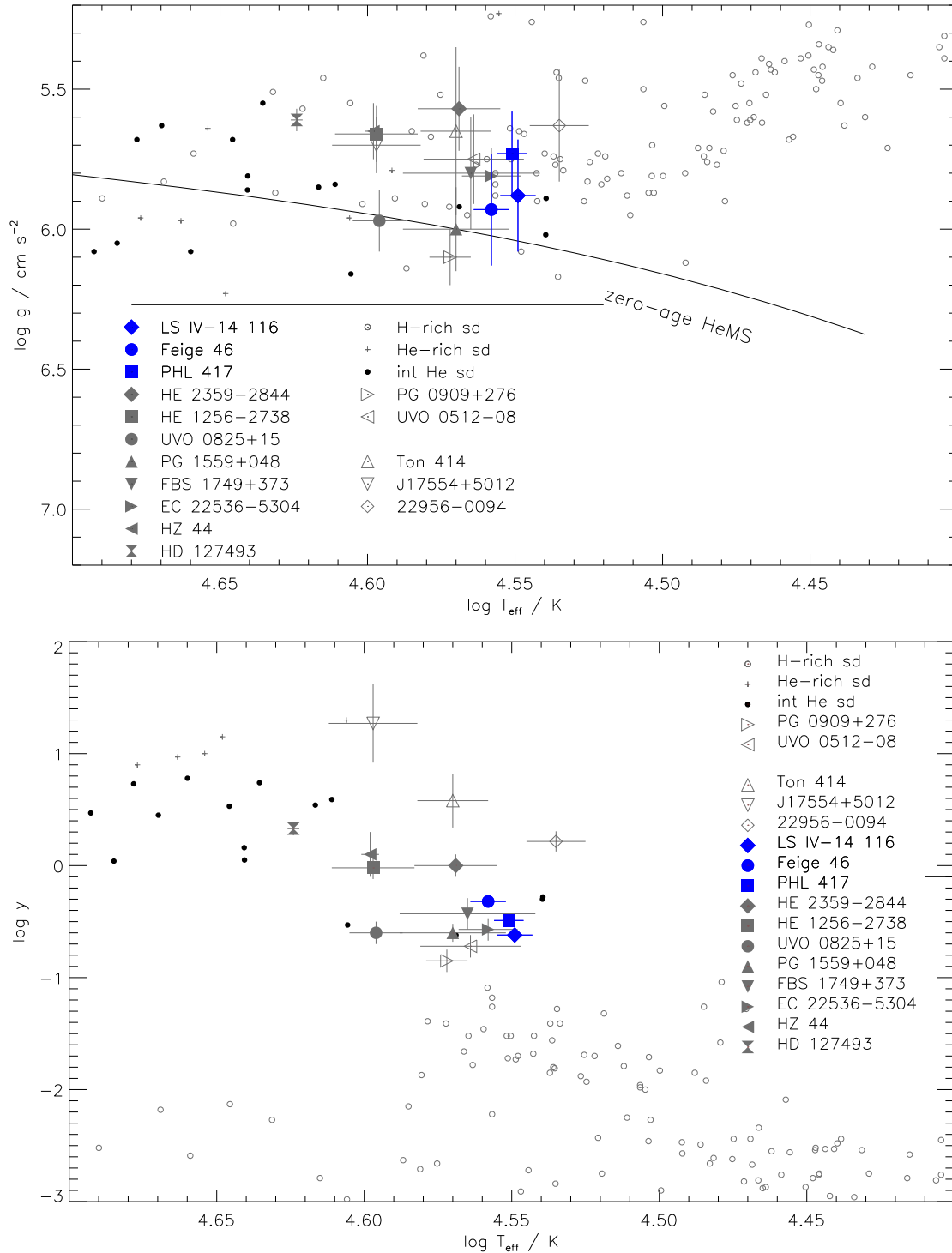


Figure 7. The distribution of V366-Aqr variables and other heavy-metal (large filled symbols), helium-rich, and normal hot subdwarfs in surface gravity (top) and helium abundance (bottom) as a function of effective temperature. The large open symbols are intermediate helium-rich subdwarfs that do not show an excess of heavy metals. The solid line shows a representative position for the theoretical zero-age helium main-sequence (HeMS; $Z = 0.02$). The data are taken from Németh et al. (2012), Naslim et al. (2013), Randall et al. (2015), Jeffery et al. (2017), Wild & Jeffery (2018), Jeffery & Miszalski (2019), Latour et al. (2019b), Dorsch, Latour & Heber (2019), Naslim et al. (2020) as well as this paper.

object as the third member of the rare group of pulsating heavy-metal stars, the V366 Aquarii pulsators.

The nomenclature is an important aspect of astronomy. We have chosen to use the variable star designation, V366 Aqr, to label the new class of pulsators, as is traditional in the variable star community. This

distinguishes the new pulsators from the hitherto recognized classes of helium-poor sdB pulsators, the short period V361 Hya, and long-period V1093 Her classes. The new class is characterized by having a spectral composition similar to the prototype, LS IV-14°116, and pulsations with periods between 0.5 and 2 h. An alternative would

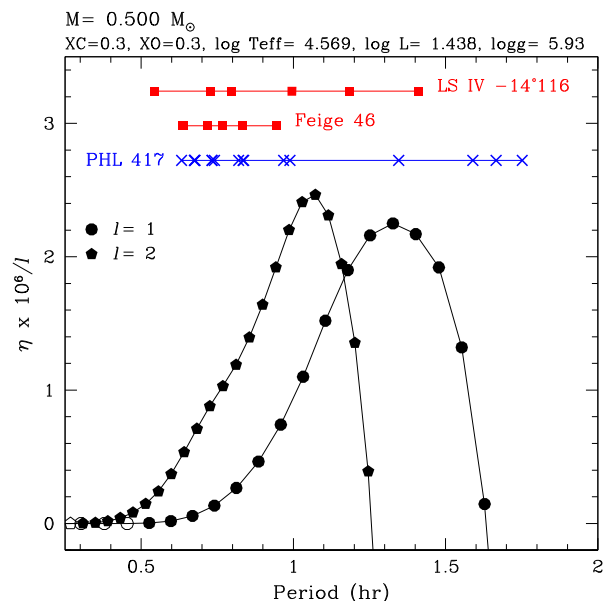


Figure 8. Growth rates η for predicted modes for a $0.50 M_{\odot}$ helium main-sequence star enriched by 30 per cent carbon and 30 per cent oxygen (by mass) are shown as a function of period. Stable modes are shown as open symbols, unstable models as solid black symbols. $\ell = 1$ and $\ell = 2$ modes are shown as circles and pentagons, respectively. The observed pulsation periods for all three Aquarids are shown and labelled.

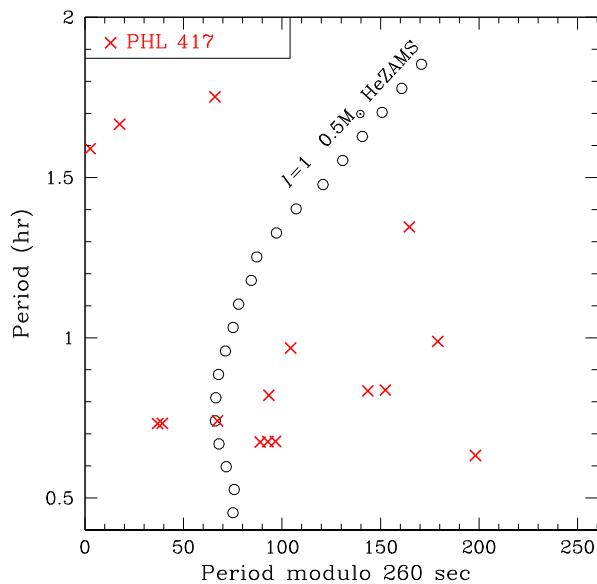


Figure 9. The Echelle diagram for $\ell = 1$ modes for the model shown in Fig. 8. Modes observed in PHL 417 are plotted as red \times .

have been to follow the pattern preferred by some of adding a V to the spectroscopic designation. But spectroscopic designations can be exceedingly complex, and often change as better observations provides a more detailed picture. For the intermediate-helium subdwarfs, the designation iHe-sdB has been used by some authors, although it should more precisely be iHe-sdOBZ, in order to recognize the presence of both He I and He II as well as heavy metals in their optical spectra. We prefer to avoid this path. The pattern used for pulsating CO white dwarfs is simpler and less ambiguous. The star

PG 1159–035 is the prototype of this spectroscopic class, and stars with similar spectra are referred to as PG 1159 stars. It was also the first star of its class to be discovered to pulsate, and given the variable star designation GW Vir. The subset of PG 1159 stars that are pulsating are therefore referred to as GW-Vir pulsators (although some authors still prefer to designate them as DOV or PNNVs). Following this pattern, we suggest that the heavy-metal stars be referred to as LS IV–14°116 stars, and pulsating members of this spectroscopic class as V366-Aqr stars.

The two K2 runs demonstrate that the pulsations are stable when comparing frequencies in observations separated by 1.5 yr, with an upper limit on \dot{P} of $1.1 \times 10^{-9} \text{ s s}^{-1}$ from the highest amplitude mode. This suggests that the interior of the star cannot be rapidly changing. The recent theoretical predictions that pulsations in heavy-metal stars are driven during an active core-helium flash event, and therefore should change with rates as high as $\dot{P} \approx 10^{-7}$ to 10^{-4} s s^{-1} is not consistent with the upper limits on period change we establish for PHL 417.

ACKNOWLEDGEMENTS

RHØ, ASB, and MDR gratefully acknowledge financial support from the Polish National Science Center under projects No. UMO-2017/26/E/ST9/00703 and UMO-2017/25/B/ST9/02218. JV acknowledges financial support from FONDECYT grant number 3160504. JJH acknowledges support by NASA K2 Cycle 6 grant 80NSSC19K0162.

This paper includes data collected by the K2 mission. Funding for the K2 mission is provided by the NASA Science Mission directorate.

The spectroscopic observations used in this work were collected at the Nordic Optical Telescope at the Observatorio del Roque de los Muchachos on La Palma, and at the Magellan Telescope at Las Campanas Observatory, Chile.

DATA AVAILABILITY

The photometric data underlying this article are in the public domain and can be accessed from the Barbara A. Mikulski Archive for Space Telescopes at mast.stsci.edu/portal/Mashup/Clients/Mast/Portal.html with either of the identifiers PHL 417 or EPIC 246373305. The spectroscopic data underlying this article will be shared on reasonable request to the corresponding author.

REFERENCES

- Ahmad A., Jeffery C. S., 2005, *A&A*, 437, L51
- Asplund M., Grevesse N., Sauval A. J., Scott P., 2009, *ARA&A*, 47, 481
- Baran A. S. et al., 2012, *MNRAS*, 424, 2686
- Battich T., Miller Bertolami M. M., Córscico A. H., Althaus L. G., 2018, *A&A*, 614, A136
- Becker S. R., Butler K., 1988, *A&A*, 209, 244
- Becker S. R., Butler K., 1989, *A&A*, 235, 326
- Becker S. R., Butler K., 1990, *A&A*, 201, 232
- Behara N. T., Jeffery C. S., 2006, *A&A*, 451, 643
- Bochanski J. J. et al., 2009, *PASP*, 121, 1409
- Butler K., 1984, PhD thesis, University College London
- Charpinet S., Fontaine G., Brassard P., Chayer P., Rogers F. J., Iglesias C. A., Dorman B., 1997a, *ApJ*, 483, L123
- Charpinet S., Fontaine G., Brassard P., Dorman B., 1997b, *ApJ*, 489, L149
- Cox J. P., 1974, *Rep. Prog. Phys.*, 37, 563
- Dorsch M., Latour M., Heber U., 2019, *A&A*, 630, A130

- Fontaine G., Brassard P., Charpinet S., Green E. M., Chayer P., Billères M., Randall S. K., 2003, *ApJ*, 597, 518
- Fontaine G., Brassard P., Green E. M., Chayer P., Charpinet S., Andersen M., Portouw J., 2008, *A&A*, 486, L39
- Gaia Collaboration, 2018, *A&A*, 616, A1
- Green E. M. et al., 2003, *ApJ*, 583, L31
- Green E. M. et al., 2011, *ApJ*, 734, 59
- Hardorp J., Scholz M., 1970, *ApJS*, 19, 193
- Haro G., Luyten W. J., 1962, *Bol. Obs. Tonantzintla Tacubaya*, 3, 37
- Heber U., 2009, *ARA&A*, 47, 211
- Heber U., 2016, *PASP*, 128, 082001
- Hibbert A., 1976, *J. Phys. B*, 9, 2805
- Huber D. et al., 2016, *ApJS*, 224, 2
- Jeffery C. S., Miszalski B., 2019, *MNRAS*, 489, 1481
- Jeffery C. S., Saio H., 2006, *MNRAS*, 372, L48
- Jeffery C. S., Hamill P. J., Harrison P. M., Jeffers S. V., 1998, *A&A*, 340, 476
- Jeffery C. S., Woolf V. M., Pollacco D. L., 2001, *A&A*, 376, 497
- Jeffery C. S., Baran A. S., Behara N. T., et al., 2017, *MNRAS*, 465, 3101
- Kilkenny D., Koen C., O'Donoghue D., Stobie R. S., 1997, *MNRAS*, 285, 640
- Kilkenny D., Worters H. L., Østensen R. H., 2017, *MNRAS*, 467, 3963
- Koen C., 1998, *MNRAS*, 300, 567
- Latour M., Green E. M., Fontaine G., 2019a, *A&A*, 623, L12
- Latour M., Dorsch M., Heber U., 2019b, *A&A*, 629, A148
- Marshall J. L. et al., 2008, in McLean I. S., Casali M. M., eds, *Proc. SPIE*, Vol. 7014, *Ground-Based and Airborne Instrumentation for Astronomy II*. Marseille, France, p. 701454
- Miller Bertolami M. M., Corsico A. H., Althaus L. G., 2011, *ApJ*, 741, L3+
- Miller Bertolami M. M., Battich T., Corsico A. H., Christensen-Dalsgaard J., Althaus L. G., 2020, *Nat. Astron.*, 4, 67
- Naslim N., Jeffery C. S., Ahmad A., Behara N. T., Şahin T., 2010, *MNRAS*, 409, 582
- Naslim N., Jeffery C. S., Behara N. T., Hibbert A., 2011, *MNRAS*, 412, 363
- Naslim N., Jeffery C. S., Hibbert A., Behara N. T., 2013, *MNRAS*, 434, 1920
- Naslim N., Jeffery C. S., Woolf V. M., 2020, *MNRAS*, 491, 874
- Németh P., Kawka A., Vennes S., 2012, *MNRAS*, 427, 2180
- Østensen R. H. et al., 2012, *ApJ*, 753, L17
- Pereira C., 2011, PhD thesis, Queen's University Belfast
- Randall S. K., Bagnulo S., Ziegerer E., Geier S., Fontaine G., 2015, *A&A*, 576, A65
- Reed M. D. et al., 2019, *MNRAS*, 483, 2282
- Saio H., Jeffery C. S., 2019, *MNRAS*, 482, 758
- Stoughton C. et al., 2002, *AJ*, 123, 485
- Telting J. H., Østensen R. H., Oreiro R., Reed M., Farris L., O'Toole S., Aerts C., 2012, in Kilkenny D., Jeffery C. S., Koen C., eds, *ASP Conf. Ser. Vol. 452, Fifth Meeting on Hot Subdwarf Stars and Related Objects*, Astron. Soc. Pac., San Francisco, p. 147
- Wiese W., Smith M., Glennon, 1966, National Bureau of Standards (USA) Pubs, I-II
- Wiese W., Smith M., Miles B., 1969, National Bureau of Standards (USA) Pubs
- Wild J. F., Jeffery C. S., 2018, *MNRAS*, 473, 4021
- Woudt P. A. et al., 2006, *MNRAS*, 371, 1497
- Yan C., Taylor K., Seaton M., 1987, *J. Phys. B*, 20, 6399

This paper has been typeset from a $\text{\TeX}/\text{\LaTeX}$ file prepared by the author.